Talanta 125 (2014) 204–209

Contents lists available at ScienceDirect

Talanta

journal homepage: www.elsevier.com/locate/talanta

Fluorescent switch for fast and selective detection of mercury (II) ions in vitro and in living cells and a simple device for its removal

Yue Yuan [a], Shenlong Jiang [c], Qingqing Miao [a], Jia Zhang [c], Mengjing Wang [a], Linna An [a], Qinjingwen Cao [a], Yafeng Guan [b], Qun Zhang [c,*], Gaolin Liang [a,*]

[a] CAS Key Laboratory of Soft Matter Chemistry, Department of Chemistry, University of Science and Technology of China, Anhui 230026, China
[b] Key Laboratory of Separation Sciences for Analytical Chemistry, Dalian Institute of Chemical Physics, Chinese Academy of Sciences, Dalian 116023, China
[c] Hefei National Laboratory for Physical Sciences at the Microscale, Department of Chemical Physics, University of Science and Technology of China, Hefei, Anhui 230026, China

ARTICLE INFO

Article history:
Received 19 January 2014
Received in revised form
25 February 2014
Accepted 25 February 2014
Available online 5 March 2014

Keywords:
Mercury (II) detection
Fluorescence switch
Selectivity
Cell imaging
Mercury (II) removal

ABSTRACT

A water-soluble, biocompatible, and fluorescent chemosensor (**1**) for label-free, simple, and fast detection of mercury ions (Hg^{2+}) in aqueous solutions and in HepG2 cells with high selectivity is reported herein. Chelation of **1** with Hg^{2+} results in the disappearance of its fluorescence emission at 350 nm and the appearance of a new emission at 405 nm. Selectivity and interference studies indicated that **1** could be selectively chelated by Hg^{2+} without interference from other metal ions. Insight into the mechanisms responsible for its fluorescence effect was gained from ultrafast transient absorption spectroscopy. With these properties, **1** was successfully applied for imaging Hg^{2+} in living cells and for removing Hg^{2+} from river water. Moreover, we also constructed a simple device for fast and effective removal of Hg^{2+} from contaminated liquid samples.

1. Introduction

Metallic mercury vapors and organic mercury derivatives (e.g., methylmercury) produce adverse effects on both environment and human health. In humans, they can seriously and permanently damage the DNA, ligand–receptor interactions, the liver, the kidney, the central nervous system, and the homeostasis of the immune system [1,2]. The long atmospheric residence time of metallic mercury vapor and its water-soluble, oxidative inorganic Hg (II) ion broadens the distribution of mercury on surface and in underground water, air, soil, and food [3]. Therefore, there is an ever-growing demand for the development of effective, selective, and practical assays for mercury detection and removal.

To date, a number of methods based on instrumental technologies have been developed for the detection of Hg^{2+}, including fluorescence spectrometry [4,5], colorimetry [6,7], ultrasensitive stripping voltammetry [8], atomic emission spectrometry [9], atomic absorption spectroscopy [10], hyper Rayleigh scattering (HRS) [11], electrochemistry [12], inductively coupled plasma mass spectrometry (ICPMS) [13], and atomic fluorescence spectrometry [14]. In recent years, fluorescent sensors for Hg^{2+} detection have been developed rapidly because of their inherent cheapness, ease of use, facility, high stability and sensitivity. Nevertheless, most fluorescent sensors for Hg^{2+} detection are based on water-insoluble organic molecules, making the detection of this water-soluble metal ion more complex and less biocompatible due to the addition of organic solvents [15–17].

In 2004, Valliant et al. reported a lysine-derived bis(pyridyl) amine, namely, a single amino acid chelator (SAAC) [18]. SAAC could be chelated with $M(CO)_3^+$ (M=Re, Tc) to form an inert complex that can be used as an amino acid for solid phase synthesis (SPPS). To structurally optimize this SAAC-type ligand so that its Re-complex is fluorescent while its ability to chelate ^{99m}Tc remains, Valliant and co-workers used N-α-Fmoc-L-lysine to react with quinoline-2-aldehyde (Q2A) in the presence of $NaBH(OAc)_3$ to yield the bifunctional ligand lysine-derived bis(quinoline) amine (SAACQ) [19]. Its Re-complex (i.e., SAACQ-Re) has fluorescent properties appropriate for in vitro microscopic studies, while its ^{99m}Tc analog could be applied to in vivo single-photon emission computed tomography (SPECT) imaging. Thus, the bifunctional ligand SAACQ could be used to simultaneously prepare complementary fluorescent and radioactive probes, allowing direct correlation between in vitro and in vivo imaging studies. SAACQ can also be used in creating libraries of structurally diverse metallopeptides, for labeling stem cells, imaging amyloid plaques or tumors, labeling biomolecules (e.g., nucleosides, carbohydrates,

* Corresponding authors. Tel.: +86 551 07935; fax: +86 551 63600730.
E-mail addresses: qunzh@ustc.edu.cn (Q. Zhang), gliang@ustc.edu.cn (G. Liang).

http://dx.doi.org/10.1016/j.talanta.2014.02.063
0039-9140

and biotin), etc. [20]. Nevertheless, the ability of SAACQ to chelate with other metal ions remains unknown.

Inspired by the pioneering studies mentioned above, in this work, we removed the hydrophobic Fmoc group from SAACQ and used the product (i.e., SAACQ-deFmoc, **1**) for the detection of metal ions in water. After numerous trials, we found that **1** can selectively and specifically coordinate with Hg^{2+}, inducing a new fluorescence emission at 405 nm. Based on these trials, we successfully employed **1** for fast and selective detection of Hg^{2+} in vitro and in living cells, and we then developed a simple device for the quick removal of Hg^{2+} from water. Recently, Aliaga and co-workers also reported one fluorescence-quenching probe for the detection of mercury (II) in aqueous media and its applications in living cells [21]. Compared with that method, our "turn-on" approach shows better sensitivity for cell imaging due to its lower interference by the background signal.

2. Experimental section

2.1. General methods

All chemicals were analytical-reagent grade or better. A Hg(II) stock solution (1000 mg L^{-1}) was purchased from J and K Chemical. Working standards were prepared by suitable dilution of the stock solution with ultrapure water. The other starting materials were obtained from Sigma or Sangon Biotech. Commercially available reagents were used without further purification, unless noted otherwise. Phosphate buffer solution (PB, 10 mM, pH 7.4) was prepared by varying the ratio from 0.01 M $Na_2HPO_4 \cdot 12H_2O$ to 0.01 M KH_2PO_4. The indicator for Hg^{2+} was made by dissolving 0.05 g diphenylcarbazone in 100 mL ethanol. Ultrapure water (18.2 MΩ-cm) was used throughout the experiment. HepG2 human liver cancer cells were supplied by the Molecular Biology Laboratory of Anhui Medical University. Cells were cultured under standard protocols in Dulbecco's modified Eagle's medium (DMEM, Hyclone) supplemented with 10% fetal bovine serum at 37 °C, 5% CO_2, and humid atmosphere. The spectra of electrospray ionization-mass spectrometry (ESI-MS) were recorded on a LTQ Orbitrap mass spectrometer (Thermo Fisher). Fluorescence emission spectra were measured with a HITACHI F-7000 FL spectrophotometer at an excitation wavelength of 312 nm. HPLC analyses were performed on an Agilent 1200 HPLC system equipped with a G1322A pump and in-line diode array UV detector using a YMC-Pack ODS-AM column, with CH_3OH (0.1% of TFA) and water (0.1% of TFA) as the eluent. ^{1}HNMR spectra were obtained using 400 MHz Bruker AV 400. Fluorescence microscopic images were taken with a fluorescence microscope OLMPUS IX71 (Japan). Inductively coupled plasma mass spectrometry (ICP-MS) was recorded on a Plasma Quad 3 ICP-MS plasma mass spectrometer (USA).

The femtosecond transient absorption data were recorded on a modified pump-probe spectrometer (ExciPro, CDP) in combination with an ultrafast amplified laser system. The pump pulses (center wavelength at 310 nm for this work; pulse energy ~8 μJ at the sample cell) were delivered by an optical parametric amplifier (TOPAS-800-fs, Coherent), which was excited by a Ti:sapphire regenerative amplifier (Legend Elite-1 K-HE, Coherent; center wavelength ~800 nm, pulse duration ~35 fs, pulse energy ~3 mJ) seeded with a mode-locked Ti:sapphire laser system (Micra 5, Coherent) and pumped with a 1-kHz Nd:YLF laser (Evolution 30, Coherent). The much weaker probe pulses (< 1 μJ/pulse at the sample cell) were provided by a stable white-light (WL) continuum (380–500 nm for this work) that was generated by focusing the 800-nm beam (split from the regenerative amplifier by a portion of ~10%) in a rotating 4.55-mm-thick CaF_2 crystal. The pump and probe beams were collinearly polarized. The instrument response function was determined to be ~100 fs by cross-correlating with the pump and probe pulses at the sample cell.

Precise spatial overlap of the pump and probe beams (with diameters of ~1 mm and 300 μm, respectively) at the center of the 1.2-mm-thick sample cell (quartz) was attained by optimizing the transient absorption signals with the aid of a laser beam analyzer (BG-USB-SP620, Ophir-Spiricon). The delays between the pump and probe pulses were varied by a motorized optical delay line (minimum step 1.56 fs; maximum delay 2.0 ns). A mechanical chopper operating at 500 Hz was used to modulate the pump pulse such that the transient absorption spectra with and without the pump pulses could be recorded alternately. The WL probe beam was first split into two tiny portions to synchronize the chopper and monitor the stability of the probe pulse using two separate photodiode detectors, and then separated into two parts (~70/30 in percentage), with the 70% part focused on the sample cell and overlapped with the pump beam yielding a transmitted probe signal, while 30% part was focused on another region of the sample cell to serve as a reference signal for achieving an optimal signal-to-noise ratio.

The sample cell was mounted on a rapidly rotating stage (5000 rpm) to ensure that the photo-excited volume of the sample was kept fresh, to avoid sample bleach during the course of the measurements. The temporal and spectral profiles of the pump-induced transient absorbance change (ΔA, in mOD; OD, optical density) were visualized with a 1024-pixel imaging spectrometer (CDP2022i) and further processed with ExiPro 2.6 software.

2.2. Synthesis and characterization of 1

After the mixture of N-α-Fmoc-L-Lysine (9.95 g, 2.7 mmol) and quinoline-2-aldehyde (9.43 g, 6 mmol) in 30 mL 1, 2-dichloroethane was stirred at room temperature for 2 h, the solution was cooled to 0 °C. Then, sodium triacetoxyborohydride (1.70 g, 8 mmol) was slowly added into the mixture. Water was added after 2 h at room temperature, and the mixture was extracted with dichloromethane (15 mL). The obtained organic layer was washed with water and brine, dried over Na_2SO_4 and concentrated under vacuum, then purified by HPLC to yield the compound SAACQ. Deprotection of SAACQ with 10% piperidine in DMF (v/v, 4 mL) at 0 °C for 20 min yielded the compound SAACQ-deFmoc (**1**) after HPLC preparation.

^{1}HNMR of compound **1** (400 MHz, DMSO-d_6) δ (ppm): 8.38 (d, J= 8.45 Hz, 2H), 8.08 (d, J=8.45 Hz, 2H), 6.91 (s, 1H), 7.96 (d, J=8.44 Hz, 2H), 7.81 (t, J=7.66 Hz, 2H), 7.64 (t, J=7.57 Hz, 2H), 7.51 (d, J=8.57 Hz, 2H), 4.81 (s, 2H), 3.95 (t, J=6.23, 1H), 3.45 (t, J=7.75 Hz, 2H), 1.94 (m, 8H), 1.59 (m, 2H) (Fig. S1); ^{13}CNMR of compound **1** (100 MHz, CH_3CN–d_3) δ (ppm): 170.15 (C1), 151.13 (C9, C9'), 144.90 (C17, C17'), 138.96 (C15, C15'), 130.90 (C12, C12'), 127.69 (C11, C11'), 127.43 (C18, C18'), 127.34 (C14, C14'), 126.85 (C13, C13'), 120.00 (C16, C16'), 57.47 (C8, C8'), 55.13 (C6), 52.07 (C2), 28.86 (C3), 23.42 (C5), 21.25 (C4) (Fig. S2); ESI-MS (m/z): $[M+H]^+$ calcd. for $C_{26}H_{28}N_4O_2$, m/z 429.23; found, m/z 429.18 (Fig. S4).

2.3. Detection of Hg^{2+} in vitro

Different volumes of Hg^{2+} (0.1 g L^{-1}) corresponding to different concentrations (0, 0.1, 0.5, 1, 5, 7.5, 10, 15, 20, 25, 30, 35, and 40 μM) were spiked into the solution of **1**. After a 1-min incubation, the fluorescence emission spectra of the solutions were obtained. Each concentration was performed three times to evaluate the standard deviation.

2.4. Detecting Hg^{2+} in living cells

After the HepG2 cells were incubated with 30 μM **1** in serum-free medium for 45 min at 37 °C, the cells were washed with PBS

for three times and then incubated with 0, 25, 50, and 100 μM Hg^{2+} in serum-free medium for 30 min at 37 °C. Then, the cells were washed with PBS another three times prior to fluorescence or differential interference contrast (DIC) imaging.

2.5. Selectivity test

Cd^{2+}, Zn^{2+}, Ni^{2+}, Na^{+}, Mg^{2+}, Li^{+}, Fe^{3+}, Fe^{2+}, Hg^{2+}, Cu^{2+}, Cr^{3+}, Co^{2+}, Ca^{2+}, K^{+}, Al^{3+}, Ag^{+}, and Pb^{2+} (20 μM) were each added to aliquots of 5 μM **1** (pH 7.4) in the presence and absence of Hg^{2+} (20 μM) for a 1-min incubation before the fluorescence emission spectra were recorded. The results were obtained from three parallel experiments.

2.6. Recovery test

Water from the Fei River (Hefei, China) was sampled and filtered with a 0.45-μm filter before use. Then, the samples were tested with the additional Hg^{2+} standards (20 μM) to evaluate the recovery of Hg^{2+}.

2.7. Hg^{2+} removal

Because SAACQ contains one Fmoc protecting group, we can readily conjugate it to the 2-chlorotrityl chloride resin beads via a covalent amide bond. Then, the SAACQ-resin beads are fully mixed with Hg^{2+}-containing water for several minutes (left), and Hg^{2+} is totally absorbed to the beads (middle). The purified water is obtained after filtration through a glass filter (right). After the activation of 2-chlorotrityl chloride resin (0.3 g, 0.33 mmol) in 5 mL N,N-Dimethylformamide (DMF), SAACQ (71.5 mg, 0.11 mmol) was conjugated to the resin in the presence of 2 eq. of N,N-Diisopropylethylamine in 2 mL DMF for 2 h. Unreacted chloride sites on the beads were then capped with methanol (26 μL) in 2 mL DMF for 5 min. After thorough deprotection of the Fmoc group from SAACQ with 20% piperidine in DMF for 3 times and measuring the amount of Fmoc using its absorbance coefficient of 5253 $M^{-1}\,cm^{-1}$ at 290 nm [22], we obtained 0.093 mmol of SAACQ resin with a coupling efficiency of 85%. Then, the SAACQ resin was divided into 5 parts, each of which was 0.01 mmol. Five water samples (2.5 mL each) containing 0.25, 0.5, 1, 2, and 4 ppm of Hg^{2+}, respectively, were mixed with the divided SAACQ resin, stirred for 5 min, and then filtered. The non-chelated Hg^{2+} in water after filtration was detected with inductively coupled plasma mass spectrometry (ICP-MS).

3. Results and discussion

3.1. Syntheses and rationale of the design

The very simple synthetic route for **1** and its coordination with Hg^{2+} are shown in Scheme 1. After deprotection of the hydrophobic Fmoc group from SAACQ with 10% piperidine, hydrophilic **1** was obtained and characterized (Figs. S1–S4). **1** offers a favorable detection environment for Hg^{2+} in water. Electrospray ionization-mass spectrometry (ESI-MS) analysis of the reaction mixture of **1** with Hg^{2+} revealed that the dominant ionic peak in the mass spectrum has a *m/z* value of 629.16, corresponding to the desired molecular weight of **1**-Hg^{2+} (Fig. S5). During the coordination of **1** with Hg^{2+}, we found that the fluorescence emission of **1** at 350 nm disappeared, and a new fluorescence emission of **1**-Hg^{2+} appeared (Fig. 1A). To quantitatively and qualitatively evaluate the chelation between **1** and Hg^{2+}, we used the fluorescence intensity ratio between 405 nm and 350 nm (F_{405}/F_{350}) for the following experiments.

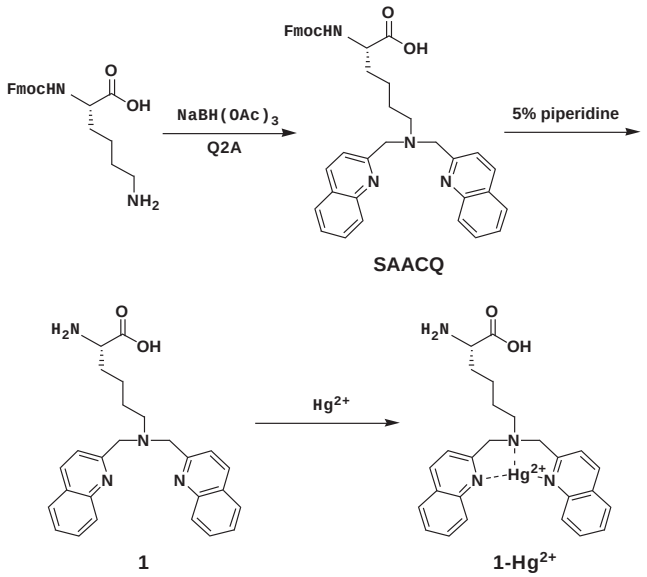

Scheme 1. Synthetic routes for **1** and 1-Hg^{2+}.

3.2. Appropriate incubation time for the chelation

First, to determine the appropriate incubation time for the chelation of Hg^{2+} with **1**, we separately added Hg^{2+} to the solution of **1** (5 μM) to reach final Hg^{2+} concentrations of 10, 20, 30, and 40 μM, respectively, at pH 7.4. The F_{405}/F_{350} values of these four groups were recorded at a time span of 1 min. All of the solutions remained stable after 1 min, suggesting a kinetically fast interaction (Fig. S6). Therefore, 1 min was chosen as the appropriate incubation time for the following analyses.

3.3. Detection of Hg^{2+} in vitro

Fig. 1A shows the fluorescence emission spectra (excited at 312 nm by a Xenon lamp) of **1** at 5 μM in the presence of various concentrations of Hg^{2+}. With increasing concentrations of Hg^{2+}, the spectra clearly show a gradual decrease of intensity at 350 nm and a gradual increase of emission intensity at 405 nm. By correlating the F_{405}/F_{350} value with the concentration of Hg^{2+}, we constructed a calibration curve for the determination of [Hg^{2+}] in vitro. As shown in Fig. 1B, a linear relationship between the F_{405}/F_{350} value and Hg^{2+} concentration ($Y=0.13091X - 0.27141$, $R^2=0.998$) was obtained over the range of 5–35 μM. The limit of detection (LOD) of Hg^{2+} in this assay was 100 nM ($S/N=3$). Following a documented method [23], we obtained the binding constant K of 4.35×10^5 M^{-1} for the chelation between **1** and Hg^{2+}, and it is comparable to those of congeneric Hg…N binding regents [24,25].

3.4. Mechanisms of fluorescence induction

To understand the mechanisms responsible for the fluorescence induction effect, one needs to examine the intrinsically fast radiationless processes detrimental to fluorescence, including internal conversion (IC), intramolecular vibrational redistribution (IVR), and intersystem crossing (ISC) [26], as schematically depicted in Fig. 2A. To this end, we performed ultrafast transient absorption measurements on both **1** and **1**-Hg^{2+} (in PBS) using a scheme featuring a femtosecond ultraviolet pump/white light continuum (WLC) probe (details in Supporting information). Upon excitation with a 310-nm (center wavelength) pumping laser, the sample molecules (**1** or **1**-Hg^{2+}) are promoted from the ground S_0

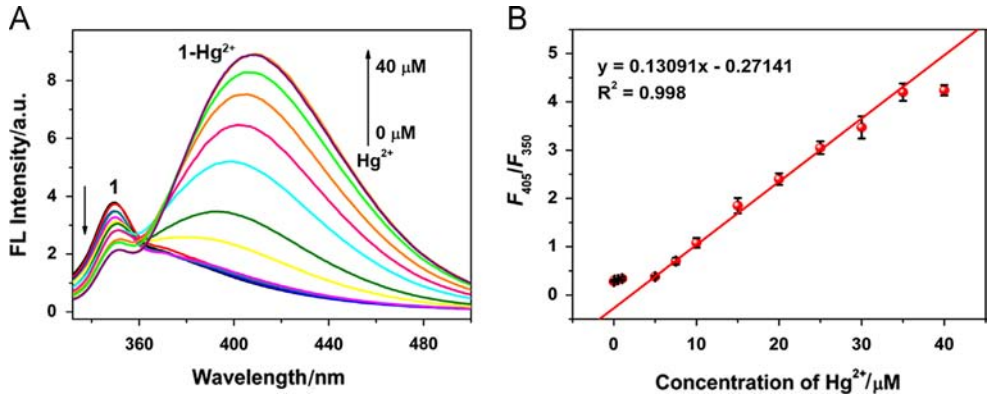

Fig. 1. (A) Fluorescence emission spectra of **1** (5 μM) in water upon the addition of various concentrations of Hg^{2+}. The concentrations of Hg^{2+} were 0, 0.1, 0.5, 1, 5, 7.5, 10, 15, 20, 25, 30, 35, and 40 μM, respectively. (B) Fitted calibration curve of the F_{405}/F_{350} values in (A) as a function of Hg^{2+} concentrations.

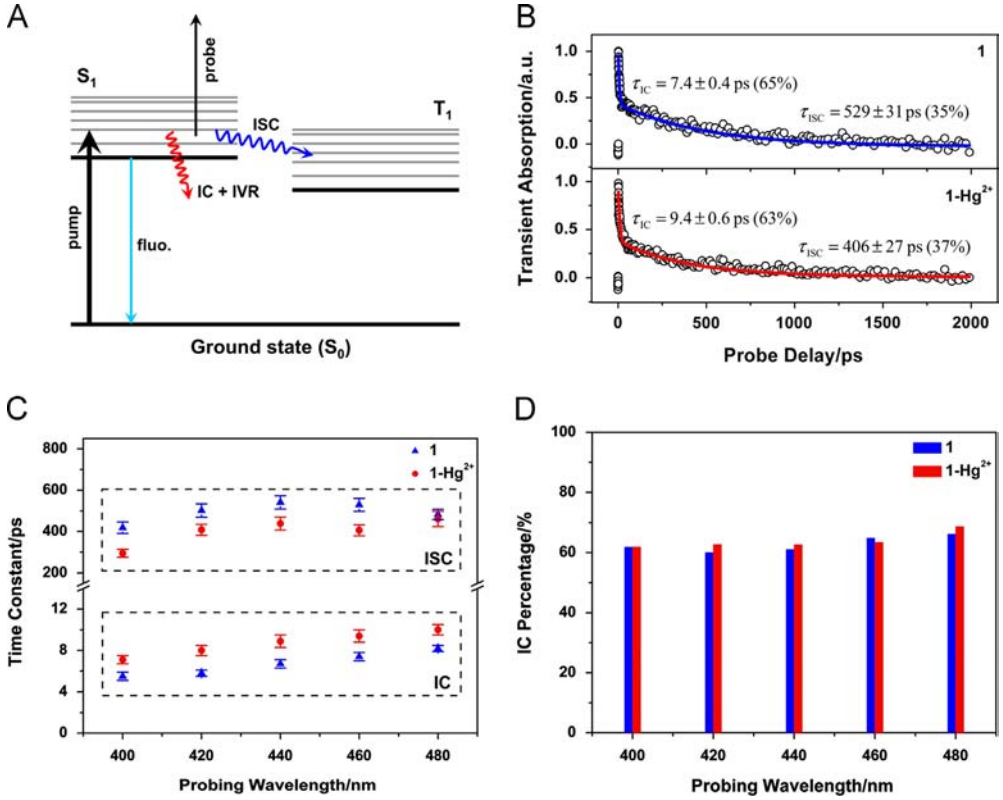

Fig. 2. (A) Schematic illustration of the involved photophysical processes, including fluorescence, IC, IVR, and ISC. (B) Typical kinetic traces (for both **1** and **1**-Hg^{2+}) probed at 460 nm when a 310-nm pump was used. (C) Relaxation time constants of IC and ISC (for both **1** and **1**-Hg^{2+}) obtained with different probing wavelengths (380–500 nm). (D) Percentage of the portion taken by IC (for both **1** and **1**-Hg^{2+}) obtained with different probing wavelengths (380–500 nm).

state to the first excited singlet S_1 state (cf. the linear absorption spectra shown in Fig. S7). The subsequent WLC probing laser (380–500 nm) follows in real time the ensuing S_1-state population relaxation by monitoring the transient absorption signals arising from the strongly allowed excited-state absorption (ESA) transitions. Most relevantly, we show here a typical comparison of the ESA kinetics, probed at 460 nm, between **1** and **1**-Hg^{2+} (Fig. 2B), which turned out to be well fitted with a bi-exponential function. The fast relaxation can be ascribed to the IC ($S_1 \rightarrow S_0$) pathway, with the slow one ascribed to the ISC from the S_1 state to the lower-lying, first excited triplet T_1 state (fitting results given in Fig. 2B). Note that, here, IC is coupled with virtually instantaneous IVR within the vibrational manifolds of S_1 state (typically on a timescale of 100 fs that cannot be well-resolved in the current experiment). Obviously, τ_{IC} (τ_{ISC}) for **1**-Hg^{2+} is larger (smaller) than that for **1**, indicating that the IC (ISC) pathway becomes less (more) efficient upon Hg^{2+} chelation. This holds also for other probing wavelengths, as exemplified in Fig. 2C, from which one can observe that upon Hg^{2+} chelation, the average variation in terms of rate (τ^{-1}) for IC (decelerated ~23%) is roughly the same as that for ISC (accelerated by ~25%). Nevertheless, the average portion taken by IC (~64%) is approximately twice that taken by ISC (~36%), as illustrated in Fig. 2D (data derived from the bi-exponential fitting of the ESA kinetics). Taken together, these results suggest that upon Hg^{2+} chelation, the efficiency decrease of IC prevails over the efficiency increase of ISC, leading to a net suppression of the fast radiationless pathways in competition with the much slower fluorescing process on the nanosecond timescale. This is consistent with the observed fluorescence induction effect. As for the accelerated ISC rate, it most likely originates from the

so-called "heavy atom effect" [27], as the ligand-to-metal charge transfer characteristic of excited states usually enhances spin–orbit coupling [28]. The IC suppression in this particular case is compatible with the fact that chelating Hg^{2+} with **1** tends to freeze (or deactivate), to a certain extent, the random motion of the two biphenyl pyridyl groups.

3.5. Specificity and recovery for Hg^{2+} detection

As shown in Fig. S8A, among these metal ions tested, only Hg^{2+} selectively responds to **1**. Fluorescence responses of **1** (5 μM) to Hg^{2+} (20 μM) in the presence of other metal ions (20 μM) were also measured (Fig. S8B), and the results indicate that the detection of Hg^{2+} is not influenced by other metal ions, even those in the same family of Hg^{2+} (i.e., Zn^{2+} and Cd^{2+}).

With the purpose of illustrating the reliability and accuracy of the assay proposed, we also used river water as a real sample for Hg^{2+} detection with **1**. As shown in Table S2 (Supporting information), the mean recovery for each sample was within the range of 99% to 103%, suggesting that this assay is applicable for Hg^{2+} detection in real-world samples.

3.6. Detecting Hg^{2+} in living cells

After the above studies, we also applied this method for detecting Hg^{2+} in living cells. As shown in Fig. 3A, fluorescence from cells treated with **1** but without Hg^{2+} is minimal. Fluorescence emission from cells treated with both **1** and Hg^{2+} increases with the increase of the concentration of Hg^{2+} added (Fig. 3B–D). These results clearly reveal that in living cells, **1** has a selective response to Hg^{2+} over other intracellular metal ions (e.g., Na^{+}, K^{+}, Ca^{2+}, Mg^{2+}, etc.) or biomolecules. Moreover, a healthy cell morphology suggests that **1** is biocompatible with cells at this concentration (Fig. S9). Differential interference contrast (DIC) images corresponding to Fig. 3 are shown in Fig. S9. The average fluorescence intensity of the HepG2 cells in Fig. 3 is measured with Image J and is summarized in Fig. S10.

3.7. Hg^{2+} removal

Considering its simplicity of synthesis, low cost, and high binding constant for Hg^{2+}, we naturally planned to use **1** to remove Hg^{2+} from water. As shown in Fig. 4, the water containing 10 μM Hg^{2+} and 55 μM **1** is colorless (number 1, left). After the addition of 20 μL of Hg^{2+}-indicator (diphenylcarbazone, 0.05%, w/v) to the 500 μL water sample containing 10 μM Hg^{2+}, color of the sample turned to be violet (number 2, middle). However, when the 500 μL water sample containing 10 μM Hg^{2+} was first treated with 55 μM **1** for 1 min, followed by the addition of 20 μL Hg^{2+}-indicator, its color remained colorless (number 3, right). These results suggest that **1** can be used to thoroughly remove the very low concentration of Hg^{2+} in water.

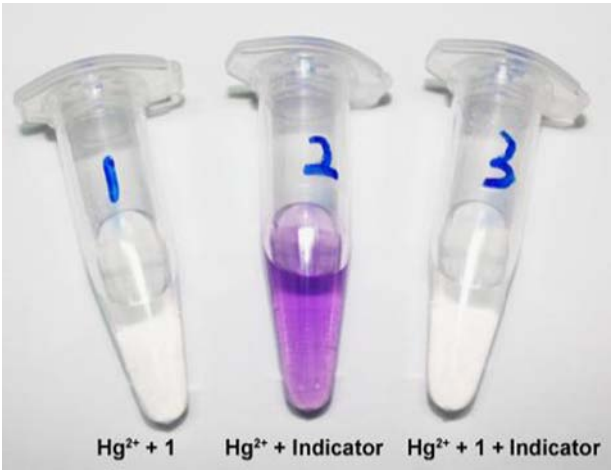

Fig. 4. Left: 500 μL of water containing 10 μM Hg^{2+} and 55 μM 1. Middle: 500 μL of water containing 10 μM Hg^{2+} and 20 ppm diphenylcarbazone, an indicator for Hg^{2+}. Right: 10 μM Hg^{2+} solution (500 μL) was incubated with 55 μM **1** for 1 min, and then 20 μL of Hg^{2+} indicator (0.05% w/v) was added, for a final concentration of 20 ppm.

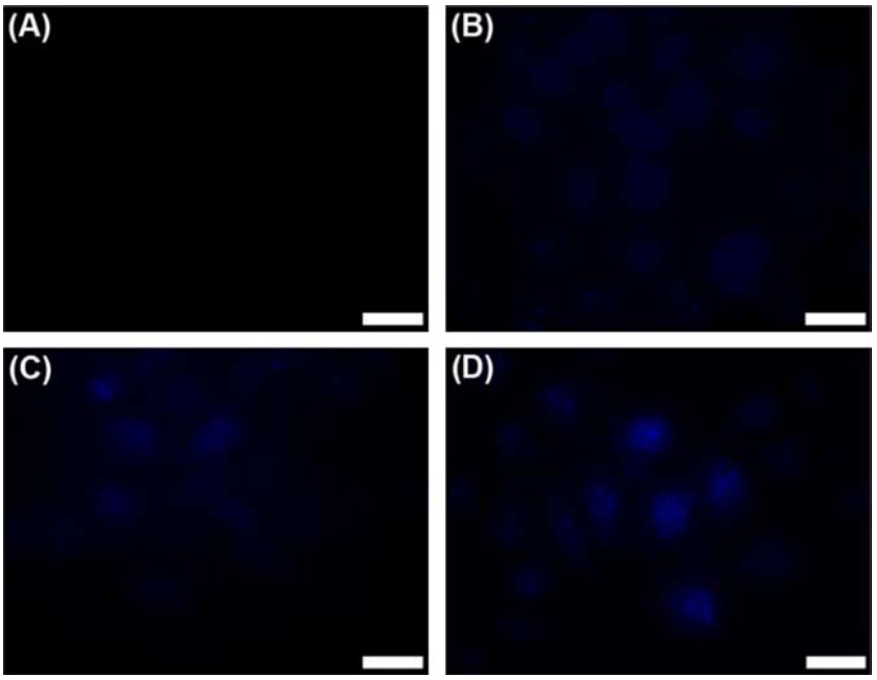

Fig. 3. Fluorescence images (DAPI channel) of HepG2 cells incubated with 30 μM **1** in serum-free medium for 45 min at 37 °C, washed with PBS for three times, then incubated with 0 μM (A, control), 25 μM (B), 50 μM (C), or 100 μM (D) of Hg^{2+} in serum-free medium for 30 min at 37 °C. The cells were then washed three times with PBS prior to imaging. Scale bars: 20 μm.

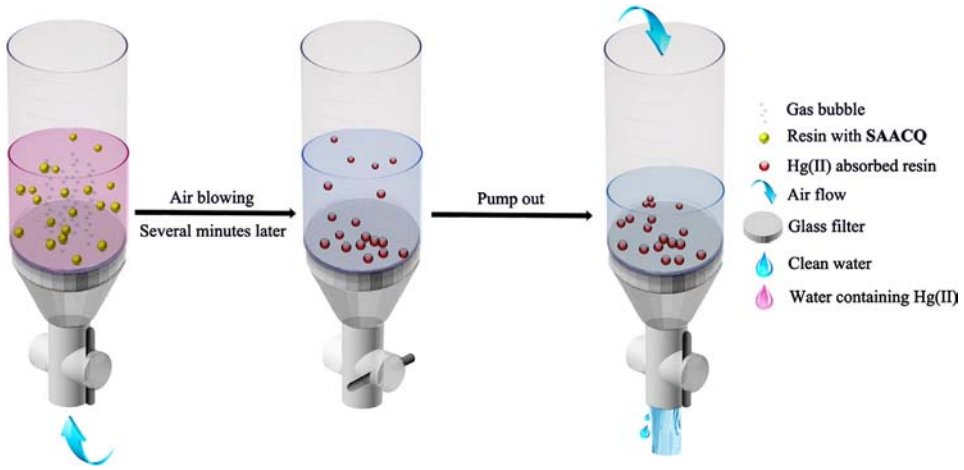

Fig. 5. Cartoon illustration of a simple device for the removal of Hg^{2+} from water.

Based on the above findings, we constructed a simple device for quick removal of Hg^{2+} from water (or other aqueous solutions), as illustrated in Fig. 5. The unchelated Hg^{2+} in water after filtration was analyzed with ICP-MS, and the results are shown in Table S3. From the ICP-MS results, one can see that our simple device has a Hg^{2+}-removal efficiency from 95% to 100% at the low Hg^{2+} concentrations from 4 to 0.25 ppm, respectively, supporting the effective Hg^{2+}-removal ability of SAACQ-resin.

4. Conclusions

In summary, we have developed a water-soluble, biocompatible, and fluorescent chemosensor for label-free, simple, and fast detection of Hg^{2+} in aqueous solution and in living HepG2 cells, with high selectivity. The mechanism underlying this detection method is based on the ICT-dependent induction of the fluorescence emission of the sensor. Insight into the fluorescence induction mechanisms was derived from ultrafast transient absorption spectroscopy. Correlation of the F_{405}/F_{350} value of the sensor with the concentration of Hg^{2+} results in a calibration curve for the determination of Hg^{2+} within 5–35 μM and a LOD of 0.1 μM in vitro. The feasibility of this assay for the detection of Hg^{2+} in living cells was also validated. Moreover, we also constructed a simple device for fast and effective removal of Hg^{2+} from contaminated liquid samples.

Acknowledgments

This work was supported by the National Natural Science Foundation of China (Grant nos. 21175122, 91127036, 21173205, and 91127942) and the Fundamental Research Funds for Central Universities (Grant WK2060190018).

Appendix A. Supporting information

Supplementary data associated with this article can be found in the online version at http://dx.doi.org/10.1016/j.talanta.2014.02.063.

References

[1] N. Langford, R. Ferner, J. Hum. Hypertens. 13 (1999) 651–656.
[2] L. Magos, T.W. Clarkson, Ann. Clin. Biochem. 43 (2006) 257–268.
[3] D.W. Boening, Chemosphere 40 (2000) 1335–1351.
[4] C.K. Chiang, C.C. Huang, C.W. Liu, H.T. Chang, Anal. Chem. 80 (2008) 3716–3721.
[5] D. Liu, S. Wang, M. Swierczewska, X. Huang, A.A. Bhirde, J. Sun, Z. Wang, M. Yang, X. Jiang, X. Chen, ACS Nano 6 (2012) 10999–11008.
[6] H. Wang, Y. Wang, J. Jin, R. Yang, Anal. Chem. 80 (2008) 9021–9028.
[7] J. Li, J. Yao, W. Zhong, Chem. Commun. (2009) 4962–4964.
[8] J. Gong, T. Zhou, D. Song, L. Zhang, Sens. Actuat. B-Chem 150 (2010) 491–497.
[9] Z. Zhu, G.C.Y. Chan, S.J. Ray, X. Zhang, G.M. Hieftje, Anal. Chem. 80 (2008) 8622–8627.
[10] M.A. Domínguez, M. Grünhut, M.F. Pistonesi, M.S. Di Nezio, M.E. Centurión, J. Agric. Food Chem. 60 (2012) 4812–4817.
[11] G.K. Darbha, A.K. Singh, U.S. Rai, E. Yu, H. Yu, P. Chandra Ray, J. Am. Chem. Soc. 130 (2008) 8038–8043.
[12] Z. Zhu, Y. Su, J. Li, D. Li, J. Zhang, S. Song, Y. Zhao, G. Li, C. Fan, Anal. Chem. 81 (2009) 7660–7666.
[13] R. Clough, S.T. Belt, E.H. Evans, B. Fairman, T. Catterick, Anal. Chim. Acta 500 (2003) 155–170.
[14] H. Bagheri, A. Gholami, Talanta 55 (2001) 1141–1150.
[15] Y. Zhao, Y. Sun, X. Lv, Y. Liu, M. Chen, W. Guo, Org. Biomol. Chem. 8 (2010) 4143–4147.
[16] J.F. Zhang, C.S. Lim, B.R. Cho, J.S. Kim, Talanta 83 (2010) 658–662.
[17] T. Schwarze, H. Müller, C. Dosche, T. Klamroth, W. Mickler, A. Kelling, H.G. Löhmannsröben, P. Saalfrank, H.J. Holdt, Angew. Chem. Int. Ed. 46 (2007) 1671–1674.
[18] K.A. Stephenson, J. Zubieta, S.R. Banerjee, M.K. Levadala, L. Taggart, L. Ryan, N. McFarlane, D.R. Boreham, K.P. Maresca, J.W. Babich, J.F. Valliant, Bioconj. Chem. 15 (2004) 128–136.
[19] K.A. Stephenson, S.R. Banerjee, T. Besanger, O.O. Sogbein, M.K. Levadala, N. McFarlane, J.A. Lemon, D.R. Boreham, K.P. Maresca, J.D. Brennan, J.W. Babich, J. Zubieta, J.F. Valliant, J. Am. Chem. Soc. 126 (2004) 8598–8599.
[20] M. Bartholoma, J. Valliant, K.P. Maresca, J. Babich, J. Zubieta, Chem. Commun. 5 (2009) 493–512.
[21] O. García-Beltrán, N. Mena, T.A. Berríos, E.A. Castro, B.K. Cassels, M.T. Núñez, M.E. Aliaga, Tetrahedron Lett. 53 (2012) 6598–6601.
[22] S.L. Mellor, C. McGuire, W.C. Chan, Tetrahedron Lett. 38 (1997) 3311–3314.
[23] R. Yang, K. Li, K. Wang, F. Zhao, N. Li, F. Liu, Anal. Chem. 75 (2002) 612–621.
[24] X. Zhang, C. Guo, Z. Li, G. Shen, R. Yu, Anal. Chem. 74 (2002) 821–825.
[25] H. Mu, R. Gong, Q. Ma, Y. Sun, E. Fu, Tetrahedron Lett. 48 (2007) 5525–5529.
[26] J.R. Lakowicz, Principles of Fluorescence Spectroscopy, Springer, New York, 2006.
[27] S.K. Lower, M.A. El-Sayed, Chem. Rev. 66 (1966) 199–241.
[28] C.C. Hsu, C.C. Lin, P.T. Chou, C.H. Lai, C.W. Hsu, C.H. Lin, Y. Chi, J. Am. Chem. Soc. 134 (2012) 7715–7724.